The effect of Ag nanoparticles on surface enhanced luminescence from Au nanovoid arrays

F. Lordan,[1] S. Damm,[1] E. Kennedy,[1] C. Mallon,[2] R.J. Forster,[2] T.E. Keyes,[2] and J.H. Rice.[1*]

[1]School of Physics, University College Dublin, Belfield, Dublin 4, Ireland.

[2]School of Chemical Sciences, Dublin City University, Dublin, Ireland.

Corresponding author

James Rice
School of Physics, University College Dublin
Belfield, Dublin
Ireland
Email: james.rice@ucd.ie
Phone: 00353 1 1762229

Key words

Nanoparticles, gold nanovoid arrays, Raman, luminescence

Abstract

Studies comparing the effect of adding two different nanoparticles compositions on the plasmonic properties of Au nanovoid arrays were undertaken. Surface enhanced resonance luminescence and surface enhanced resonance Raman studies comparing dispersed Ag nanoparticles and Ag nanoparticle aggregates on gold nanovoid arrays were undertaken. These studies showed that using Ag nanoparticle aggregates increased the both luminescence and Raman efficiency relative to when dispersed nanoparticles were used, in addition these studies also showed that adding dispersed Ag nanoparticles supported a more reproducible enhancement in luminescence and Raman across the substrate compared to using Ag nanoparticle aggregates. Finite element analysis simulations indicated that surface plasmon polariton distribution in the sample was affected by the presence of the Ag nanoparticles on the Au nanovoid array.

Introduction

A considerable amount of research has been undertaken to advance the understanding of optical processes in molecular- or nano-materials such as quantum dots, nanodisks, fullerenes and carbon nanotubes [1-9]. Optical spectroscopy and microscopy techniques such as Raman and fluorescence based methods provide a way to potentially analyse both the optical and structural properties of such materials [2-11]. Methods that can increase the emission or Raman signal intensity can lead to increased analytical sensitivity. One approach to enhance fluorescence or Raman signal strength is to use plasmon active substrates. Metal enhanced

luminescence or metal enhanced Raman potentially enhances the signal from the target system, such methodology is referred to as surface enhanced luminescence (SEL) or surface enhanced Raman scattering (SERS). One approach to generate SEL and SERS is to use spherical metallic nanoparticles (NPs) or roughened metallic surfaces to generate a plasmon active substrate [12-14]. These nanoscale materials are predicted to enable signal enhancement up to 10^{10} for SERS [15]. The origin of such high enhancements have been attributed to hotspots occurring on the surface of the substrate [15]. The occurrence of such localised "hotspots" is variable, as there is a lack of complete control over the size and shape of metallic particles/features formed. This leads to irreproducibility of the SEL or SERS signal. Methods using lithography such as electron beam based approaches have been used to create reproducible plasmon active surface features. However the high costs associated with this approach have prevented wide scale use.

Reproducible plasmon active substrates based on nanosphere lithographic fabrication methods have been reported. The resulting structures have nanovoid architecture such as those reported here. These nanovoid structured surfaces possess spherical cap architecture and are arranged uniformly in a hexagonally close-packed array [16-25].

Localised surface Plasmon polaritons (LSPPs) exist inside the nanovoid and localised and delocalised (propagating) surface Plasmon polaritons (PSPPs) exist on the flat surface of the sample [17-19]. Several studies have been reported demonstrating SERS using nanovoid substrates [17-24]. Baumberg et al [22] showed strong correlations between plasmon resonances and Raman enhancements by studying different void dimensions as a function of incident angle. Studies of nanovoid samples coated with organic semiconducting molecular J-aggregate films have been undertaken [23]. This study showed room temperature excitonic luminescence is enhanced by plasmonic coupling using nanovoid substrates. Studies of the emission of dye absorbed to the surface of nanovoids have been carried out [19-21].

Nanovoid array substrates are commonly made from Ag or Au as such materials produce chemical and structurally stable arrays with visible and NIR plasmonic absorbance. Au is often used to create such nanostructures as it provides significant enhancement and produces more stable arrays than Ag due to its chemical inertness [18]. Ag arrays provide larger enhancements but tend to be of lower quality than those made of Au. Combining both Au and Ag into single nanostructured substrates has been the topic of some studies in which a Ag or Au layer was placed over a Au structured surface. This reported enhancements in SERS signal [18, 24]. Huang et al [24] investigated the field enhancement gained when an Au NP was placed inside an Au nanovoid at a range of distances from the curved inner surface of the void. Following this Speed et al [26] studied the effect of Ag NPs added to an Au substrate on the SERS signal of adsorbed 4-mercaptoaniline and 4-mercaptobenzoic acid. This study showed a significant enhancement in the SERS signals of the adsorbates and was attributed mainly to the electromagnetic hotspot formed in between the Au substrate and Ag NPs. Ross et al [27] looked at the possibility of placing Au NPs in Au cavities and using these structures as a plasmonic antenna array. This plasmon enhanced void-particle provided a significant increase in both hot-spot density and intensity. To date no study has been reported on the effect of different compositions of Ag NP on SEL from nanovoid array substrates. We study here Au nanovoid arrays with a self-assembled monolayer of a luminescent dye [Ru(bpy)2(Qbpy)]2+ adsorbed to its surface. SEL studies, along with surface enhanced resonance Raman (SERR), were undertaken examining the effect of adding dispersed nanoparticles (NPs) and aggregated Ag nanoparticles (agg-NPs) to the plasmonic properties of a gold nanovoid array substrate.

Experimental

The Au nanovoid array was produced by electrodeposition of Au through an array of self-assembled 600nm diameter polystyrene spheres on gold modified silicon wafer. The resulting array was then modified with a monolayer of [Ru(bpy)2(Qbpy)]2+ as outlined previously [19]. Atomic force microscopy (AFM) was carried out on the unmodified nanovoid array to confirm the pitch and depth of the cavities, see Fig. 1. These studies showed that the cavities are arranged in a regular hexagonal array with a centre to centre pitch of 615nm, consistent with the fact that 600nm diameter polystyrene beads were used as a mask. The cavities were found to have a depth of approximately 150nm, giving them a normalised thickness value (depth/diameter) of 0.25.

Ag NPs were prepared by following the guidelines set out by Ratyakshi and Chauhan [28]. These were left aside for approximately 2 months to allow aggregates (agg-NP) to form. The solution changed from a clear yellow colour (see Fig. 1b) to an opaque grey colour and the absorption spectrum broadened signifying formation of aggregates (see Fig. 1c) over this time frame. The optical absorption spectra (shown also in Fig 1b and c) show that for agg-NP are broader red shifted peak is seen compared to dispersed NPs. The Au nanovoid array was divided into four pieces. Two pieces were left unmodified, Ag NPs were adsorbed to the third piece and agg-NPs were added to the fourth piece. These were deposited by leaving the nanovoid substrates submerged in the aqueous Ag solutions for 2 hours. The substrates were removed and rinsed with purified water to remove excess Ag. The samples were then left to dry before measurements were taken.

A 532nm laser was used to excite the [Ru(bpy)2(Qbpy)]2+adsorbed to the samples. SEL was recorded along with Raman. The Raman scatter in this work is referred to as surface enhanced resonance Raman scattering (SERRS) as the laser line at 532nm overlaps with the absorption curve of [Ru(bpy)2(Qbpy)]2+. Scatter was collected through a lens and focussed onto a slit in the spectrometer window. Signals were then detected by a CCD and displayed using Andor Solis software. SERRS and SEL signals were collected from both the modified and unmodified samples.

Results and discussion

AFM studies of nanovoids with and without agg-NPs were undertaken, shown in Fig 1. Measurements were carried out on both the modified and unmodified samples to check for the presence of aggregates. Line profiles of the unmodified nanovoid array showed smooth topography with no local roughness. Due to this, the presence of aggregates was detected as a consistent increase in topographical roughness on the modified side. Histogram analysis of the arrays' z-heights was performed in order to assess aggregate presence and size. The results of these studies are shown in Fig 2. Force gradient maps which correspond to the derivative of height at each point for the unmodified array and the modified array are shown in Fig 1, both over an 800nm area. Comparison of this surface mapping shows a qualitative increase in roughness on the nanovoid sample surface following deposition of the agg-NPs. Fig 2 shows the unnormalised roughness histograms for 3000 randomly chosen points on the array alone (grey) and the array with aggregates (yellow). The broadening of the roughness parameter on the modified side is evidence of aggregate presence. Moreover, subtraction of the pristine control array roughness distribution from the aggregate side histogram yields the distribution of aggregate heights, the magnitude of which is shown in the inset of Fig 2. The

agg-NP aggregates are primarily in the range of 30 – 60nm in height. AFM studies for the NPs deposited on the nanovoid array showed NP size values of 10-40nm.

SERR and SEL were recorded simultaneously from the nanovoid array sample, an example is shown in Fig 2 along with a more detailed SERRS spectrum with peak positions marked. Fig 3 summarises the SEL and SERRS signals obtained from the Au nanocavities and gold film, both with and without Ag NP deposition. Fig 3a shows SERRS signals from the Au nanovoid array with and without deposited NPs. The spectra in red show the signals obtained from the unmodified sample and the black plots represent the signals obtained from the Ag modified sample. The addition of NPs leads to an increase in the Raman scattering efficiency. There is approximately a 4 fold increase in SERRS scattering intensity when NPs are added. The probe dye was also prepared on an Au film with NPs deposited. The data from this sample is plotted in Fig. 3b. The red plot represents the signal obtained from the gold film alone. No Raman is visible. After deposition of NPs the Raman signal becomes clear (the black plot) with a maximum count of approximately 5200. The data from both the nanostructured and flat gold showed in Figs 3a and 3b shows that SERRS signals in both cases are increased with NP deposition. Figs 3c and 3d show the simultaneous SERRS and SEL spectra obtained from the nanocavity array and from a gold film respectively, both with and without NP deposition. In both spectra the red plots represent the signal without NP deposition and the black plot represents the signal with NP deposition. SEL is increased for the probe molecule following the addition of NPs when a nanovoid substrate is used while no increase in SEL is seen for flat gold. This suggests that on the gold film the NPs are in close proximity to the probe molecule i.e. < 5 nm which would mean a reduction in SEL and consequently an increase in SERRS signal intensity would be expected which is what is observed. This indicates that the geometry of the nanovoid substrate enables conditions for SEL enhancement i.e. a significant number of probe molecules are placed c.a. 5 nm in distance from the NPs. Separation distances below this value are reported to result in significant quenching of the luminescence signal [29] For optimum SERRS (or SERS) the NP would need to be in close contact with the probe molecule. This suggests that the geometry of the nanovoid allows for both possibilities of SERRS and SEL enhancement to occur.

Fig 4a shows SERRS signals from the Au nanocavity array with and without agg-NP deposition. Deposition of agg-NPs leads to approximately a 6-fold increase in SERRS signal. The red plot in Fig 4b represents the spectrum from a gold film alone, there is no discernible SERRS signal. Deposition of agg-NPs leads to a clear SERRS signal with a maximum count of approximately 5540 counts. Fig 4c shows the simultaneous SERRS and SEL spectra obtained from the nanocavity array both with and without agg-NP deposition. After deposition of agg-NPs the SEL signal stays approximately the same but the shape is changed significantly. This is in contrast to the SEL signal obtained from the Au nanocavity array with NP deposition in which the SEL signal was enhanced. The deposition of NPs supports enhanced luminescence while the deposition of agg-NPs seems to increase luminescence quenching leaving the signal intensity very slightly increased. The addition of NPs does not remove the luminescence band feature to the same extent as deposition of agg-NPs.

The variation in SEL and SERRS signal intensity over the NP deposited nanovoid substrate surface was investigated by probing multiple areas of the substrate and recording the resulting SEL/SERRS signal intensities at each spot. Fig 5a shows a compilation of the SEL and SERRS spectra recorded from the Au nanocavities with deposited NPs. Data showed that the intensity of the luminescence at 1.86eV has an average value of 325 counts with a standard deviation of 38 counts. Inset is a scatter plot of the values recorded at 1.86eV for the

luminescence. The narrower spectrograph window was then used to record a kinetic series of spectra, hereby referred to as KS, ie consecutively recorded spectra, where each spectrum was recorded over a different area of the substrate of the SERRS signal, see Fig. 5b. Data showed that the intensity of the Raman peak at 1610cm^{-1} had an average value of 264 counts with a standard deviation of 20 counts. Inset in Fig 5a is a scatter plot of the values of the peak.

This consistency of the SERRS and SEL signals across the agg-NP modified samples was also investigated. Fig 5c shows a compilation of the SEL and SERRS spectra recorded from the Au nanocavities with deposited agg-NPs. Data showed that the intensity of the luminescence at 1.86eV has an average value of 2198 counts with a standard deviation of 482 counts. Inset is a scatter plot of the values recorded at 1.86eV for the luminescence. The narrower spectrograph window was then used to record KS spectra of the SERRS signal, see Fig. 5d. Data showed that the intensity of the Raman peak at 1610cm^{-1} had an average value of 308 counts with a standard deviation of 118 counts. Inset in Fig 5a is a scatter plot of the values of the peak. These studies show that both the SERRS and SEL signals are more consistent over the sample with NP deposition than the sample with agg-NP deposition. The effect of Ag deposition on the ratio of the SERRS intensity to the intensity of the luminescence signal was investigated. This was carried out by examining a number of different sites across the sample to assess the variation in SERRS/SEL relative intensities. SERRS/SEL signal intensities for nanovoids with deposited NPs showed that the average ratio of Raman to luminescence signals was 1.21 with a standard deviation of 0.11. These values were extracted from KS studies of the Raman and luminescence signals from across the active area on the sample. Studies of SERRS/SEL signal intensities for nanovoids with deposited agg-NPs showed that the average ratio of Raman to luminescence signals was 1.84 with a standard deviation of 0.32. Addition of agg-NPs to the nanocavity array increases the SERRS/SEL ratio more than the addition of NPs, due to the increased quenching effect on the luminescence.

Simulations using COMSOL were undertaken to assess the impact of agg-NPs on Au nanovoid structures. For the simulations Finite Element Method (FEM) was used. All the simulations were done in 2D with a p-polarized electromagnetic plane wave hitting the void at normal incidence. The dielectric functions for gold and silver were taken from Johnson and Christy [30] A 20 nm Ag disc was used to represent a dispersed NP, a 60 nm sphere represents an agg-NP particle. These NP sizes were derived from scanning probe microscopy studies and from optical absorption spectra (shown in Fig 1) peak positions. The NP was then placed inside a nanovoid at varying distance from the bottom of the nanovoid.

Fig 6 shows the simulations carried out for a 20nm NP in an Au nanocavity and also on Au film. Fig 6a shows the different positions (marked numerically 0 to 3) at which the NP was placed inside the nanovoid structure. These are the points at which the electric field values (E-field) were taken. Simulation studies examining the E-field intensity as a function of wavelength (hereby referred to as E-field spectra) for the 20nm NP on the Au film show the E-field spectra intensities depend on the sphere-film separation distance (see Fig 6b) at a given point. The highest E-field is seen for a separation distance of 0.3nm. The E-field intensities was simulated at point 2. The E-field intensity decreases with increasing separation distance from 0.3nm to 1nm. A similar trend is seen in Fig 6c for the NP in the Au nanocavity.

Figs 7b and 7c show the same calculations for a 60nm NP used to represent an agg-NP. Again the simulations for the The E-field spectra (Fig 7b) for the Ag NP on the Au film show features that depend on the sphere-film separation distance, with the highest E-field recorded for a separation distance of 0.3nm for both the NP-nanocavity and the NP-Au film systems (Figs 7b and 7c). Comparing Figs 6b and 6c for the dispersed NP with 7b and 7c for the agg-NP it is shown in the plots that the E-field strength is greater for the case with the 60nm NP (agg-NP) in agreement with experimental studies (see above).

Figs 6d and 7d show the E-field values calculated at all four points at a constant separation distance d=0.3nm for both NP sizes. This separation distance consistently gave the highest E-field values across all four points. The plots in Figs 6d and 7d show that for a constant separation distance d=0.3nm point 2 gives the highest enhancement for both the Au film and the nanocavity across the whole wavelength range in the case of a 60nm NP. In the case of the 20nm NP both points 1 and 2 give the highest enhancements. In comparison a separation distance of 1nm (Figs 6e and 7e) consistently gave the lowest E-field values for both NP sizes. For this configuration the highest E-field enhancement is seen at point 1 for the 60nm NP and at point 0 for the 20nm NP both the Au film and the nanocavity across the whole wavelength range. These plots show that the position of the highest E-fields are dependent on the NP-nanocavity/film separation distance and that the E-field values vary as detection points are moved across the gap between the NP and cavity/film. They also illustrate that the NP-nanocavity system is quite complex, with E-field values changing significantly for small changes in the separation distance and for small shifts in detection points. These simulations show that the nature of the substrate i.e. void or flat gold, and the separation distance between the substrate and NPs significantly affect the plasmonic properties.

The plots for the 60nm NP are more complex than those for the 20nm NP as a second mode becomes apparent, this is the NP mode. Only the D mode is visible in the spectra for the smaller NP. 23 Two particular points of interest are looked at; 580nm and 670nm which represent the location of the observed Raman (λ_{Raman}=580nm) and luminescence (λ_{lum} = c.a. 670nm) respectively. For the 20nm NP the maximum enhancement at 580nm occurs at point 1 with a separation distance of d=0.3nm. Looking for the maximum enhancement for the luminescence at 670nm, it can also be seen at point 1 with a separation distance of 0.3nm. However at this distance fluorescence quenching is extremely significant and accounts for the less intense experimental luminescence spectra obtained from the agg-NP deposited sample [29]. The NP nanovoid distance is too small for effective SEL. The energy within the molecules, generated by illumination, will be transferred to the metals instead of being emitted as a photon. The electric field values are higher at 580nm than at 670nm as λRaman coincides with the D of the cavity. Switching now to the plots for the 60nm NP, the NP mode can be clearly seen at a lower wavelength than the D mode. The maximum electric field enhancement occurs with a separation distance of 0.3nm at point 2. The case is the same for the luminescence, again with a higher electric field value at λ_{Raman}.

Conclusion

The nanovoid + NP/agg-NP samples have areas with silver deposition both on the surface between the cavities and within the cavities. The enhancement field is a combination of the fields generated from single/few nanoparticles within the void, a filled void, NPs on the surface between the cavities and empty unfilled cavities. Experimentally the largest enhancement is seen for SERRS from the nanocavity substrate with deposited agg-NPs, this is consistent with the COMSOL calculations carried out above. The presence of voids

without any silver and the presence of the probe molecule on gold between the nanovoids cannot be discounted in contributing to the observed SEL and SERRS signal. However studies of different regions of the nanovoid sample following the addition of NPs or agg-NPs show that there is a reasonably constant SEL signal response across the sample, with less variation for both the SERRS and SEL signals from the sample with deposited NPs.

Acknowledgements

The authors would like to thank Science Foundation Ireland (SFI) for supporting this work.

References

1. J.C. Charlier 2002 Defects in Carbon Nanotubes. Account.Chem. Research, 35 (12): 1063.

2. J.H. Rice, J.W. Robinson, A. Joujour, R.A. Taylor, R.A. Oliver, G.A.D. Briggs, M.J. Kappers, C.J. Humphreys 2004 temporal variation in optical transitions from single InGaN quantum dots. Applied Physics Letters 84: 4110-41104

3. R.A. Taylor, J.W. Robinson, J. H. Rice, A. Jarjour, J. D. Smith, R. A. Oliver, G.A.D. Briggs, M. J. Kappers, C. J. Humphreys, and Y. Arakawa 2004 dynamics of single InGaN quantum dots. Physica E 21: 285-288

4. J. H. Rice, J. P. Galaup, and S. Leach 2002 fluorescence and phosphorescence spectroscopy of C70 in toluene solid solution at 5K: Switching of character for the lowest lying state Chem. Phys. 279(1): 23

5. R.W. Martin, P.R. Edwards, J.H. Rice, J.W. Robinson, A. Joujour, R.A. Taylor, R. Oliver, G.A.D. Briggs 2005 luminescence properties of isolated InGaN/GaN quantum dots Phys. Stat. Sol. A 202(3): 372

6. J. H. Na, R. A. Taylor, J. H. Rice, J. W. Robinson, K. W. Lee, Y. S. Park, C. M. Park, T. W. Kang 2005 time-resolved and time-integrated photoluminescence studies of coupled asymmetric GaN quantum discs embedded in AlGaN barriers Appl. Phys. Letts. 86(8): 083109

7. J.H. Rice, R. Aures, J.P. Galaup, S. Leach 2001 fluorescence spectroscopy of C60 in toluene at 5K Chemical Physics 263: 401-414

8. N.C. Carville, M. Manzo, S. Damm, M. Castiella, L. Collins, D. Denning, S.A.L. Weber, K. Gallo, J.H. Rice, B. J. Rodriguez 2012 Photoreduction of SERS-active metallic nanostructures on chemically-patterned ferroelectric crystals ACS Nano 6(8): 7373

9. J. H. Na, R. A. Taylor, J. H. Rice, J. W. Robinson, K. W. Lee, Y. S. Park, C. M. Park, T. W. Kang 2005 , two-dimensional exciton behavior in GaN nanocolumns grown by molecular-beam epitaxy Appl. Phys. Letts. 86(12): 123102

10. J.H. Rice 2007 fluorescence microscopy beyond the diffraction limit: fluorescence imaging with ultrahigh resolution. Molecular BioSystems 3: 781 - 793

11. G. Hill, J.H. Rice, S.R. Meech, P. Kuo, K. Vodopyanov, M. Reading 2009 nano-Infrared surface imaging using an OPO and an AFM. Optics Letters 34: 431–433

12. S. Nie, and S. Emory 1997 Probing Single Molecules and Single Nanoparticles by Surface-Enhanced Raman Scattering. Science 275(5303): 1102

13. N. Al-Alttar, E. Kennedy, I. Kopf, S. Giordani, J.H. Rice 2012 Surface-enhanced Raman scattering from small numbers of purified and oxidised single-walled carbon nanotubes, Chem. Phys. Lett. 535: 146-151

14. K. Kneipp, K. Wang, H. Kneipp, L. Perelman, and I. Itzkan Single molecule detection using surface-enhanced Raman scattering (SERS) Physical Review Letters 78: 1667-1670

15. H. Xu, J. Aizpurua, M. Kall, P. Apell 2000 Electromagnetic contributions to single-molecule sensitivity in surface-enhanced Raman scattering Phys. Rev. E 62(3): 4318

16. B. Jose, R.Steffen, U.Neugebauer, E. Sheridan, R. Marthi, R. J. Forster, T. E. Keyes 2009 Emission enhancement within gold spherical nanocavity arrays Phys. Chem. Chem. Phys. 11(4): 10923

17. T. A. Kelf, Y. Sugawara, R. M. Cole. J. J. Baumberg, M. E. Abdelsalam, S. Cintra, S. Mahajan, A. E. Russell, P. N. Bartlett 2006 Localized and delocalized plasmons in metallic nanovoids Phys. Rev. B. 74(24): 245415

18. E. Cortes, N. G.Tognalli, A. Fainstein, A. M. Vela, R. C. Salvarezza 2009 Ag-modified Au nanocavity SERS substrates Phys. Chem. Chem. Phys. 11 (34): 7469

19. F. Lordan, J. H Rice, B. Jose, R. J. Forster, and T. E. Keyes 2010 Surface enhanced resonance Raman and luminescence on Plasmon active nanostructured cavities. Appl. Phys. Letts. 97 (15): 153110

20. F. Lordan, J. H Rice, B. Jose, R. J. Forster, T. E. Keyes 2011 Site selective surface enhanced Raman on nanostructured cavities. Appl. Phys. Letts. 99 (3): 033104

21. F. Lordan, J. H Rice, B. Jose, R. J. Forster, T. E. Keyes 2012 Enhanced fluorescence from nanostructured cavities , J. Phys. Chem. C 116 (2): 1784

22. J. J. Baumberg, T. A. Kelf, Y. Sugawara, S. Cintra, M. E.Abdelsalam, P. N. Bartlett, A. E. Russell 2005 Angle-Resolved Surface-Enhanced Raman Scattering on Metallic Nanostructured Plasmonic Crystals. Nano Letts. 5(11): 2262

23. Y. Sugawara, T. A. Kelf, J. J. Baumberg, M. E. Abdelsalam, P. N. Bartlett 2006 Strong Coupling between Localized Plasmons and Organic Excitons in Metal Nanovoids. Phys. Rev. Letts. 97 (26): 266808

24. F. M. Huang, D. Wilding, J. D. Speed, A. E. Russell, P. N. Bartlett, J. J. Baumberg 2011 Dressing Plasmons in Particle-in-Cavity Architectures. Nano Letts. 11(3): 1221

25. F. Lordan, N. Al-Attar, C. Mallon, J. Bras, G. Collet, R.J. Forster, T.E. Keyes, J.H. Rice 2013 temperature dependence of a1 and b2 type modes in the surface enhanced Raman from 4-Aminobenzenethiol. Chem. Phys. Lett. 556: 158–162

26. J. D. Speed, R. P. Johnson, J. T. Hugall, N. N. Lal, P. N. Bartlett, J. J. Baumberg, A. E. Russell 2011 SERS from molecules bridging the gap of particle-in-cavity structures. Chem. Comm. 47(22): 6335

27. B. M. Ross, L. P. Lee 2009 Creating high density nanoantenna arrays via plasmon enhanced particle–cavity (PEP–C) architectures. Opt. Express 17(8): 6860

28. R. Ratyakshi, R. Chauhan 2009 Colloidal Synthesis of Silver Nano Particles. Asian Journal of Chemistry 21(10): 113

29. K. Aslan, I. Gryczynski, Malicha, E. Matveeva, J. R. Lakowicz, C. D. Geddas 2005 Metal-enhanced fluorescence: an emerging tool in biotechnology. Currnet Opinion in Biotechnology, 16(1): 55

30. P. B. Johnson, R. W. Christy 1972 Optical Constants of the Noble Metals. Phys. Rev. B 6(12): 4370

Figures

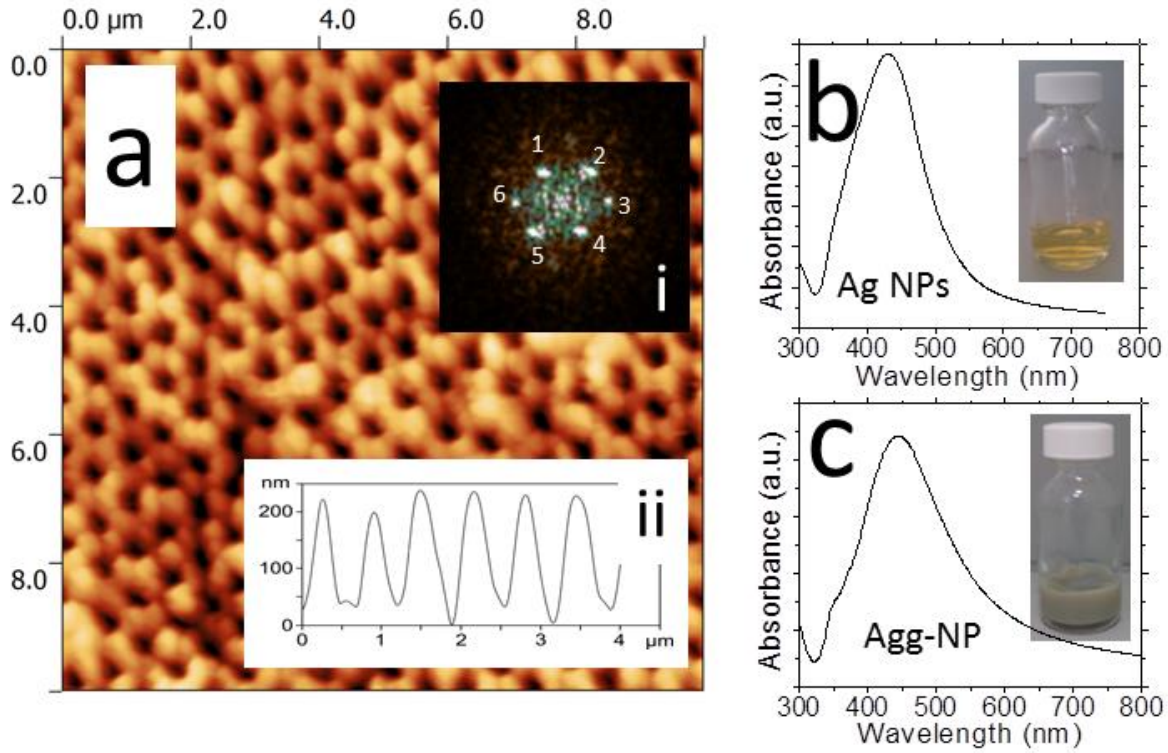

FIG. 1 (a) AFM topography image of the array, with a 2D Fast Fourier Transform (FFT) inset i) in the top right corner illustrating hexagonal regularity. The mean distance of 1-6 in the 2D FFT to the centrepoint corresponds to an array periodicity of 615nm. Inset ii) is a line profile of the array showing a depth of approximately 150nm. (b) Ag NP solution showing the characteristic pale yellow colour. UV-Vis spectrum of the Ag NPs in aqueous solution with a characteristic peak at 430nm. (c) Ag aggregates solution shown. UV-Vis spectrum of the Ag aggregates in aqueous solution with a broader absorption peak.

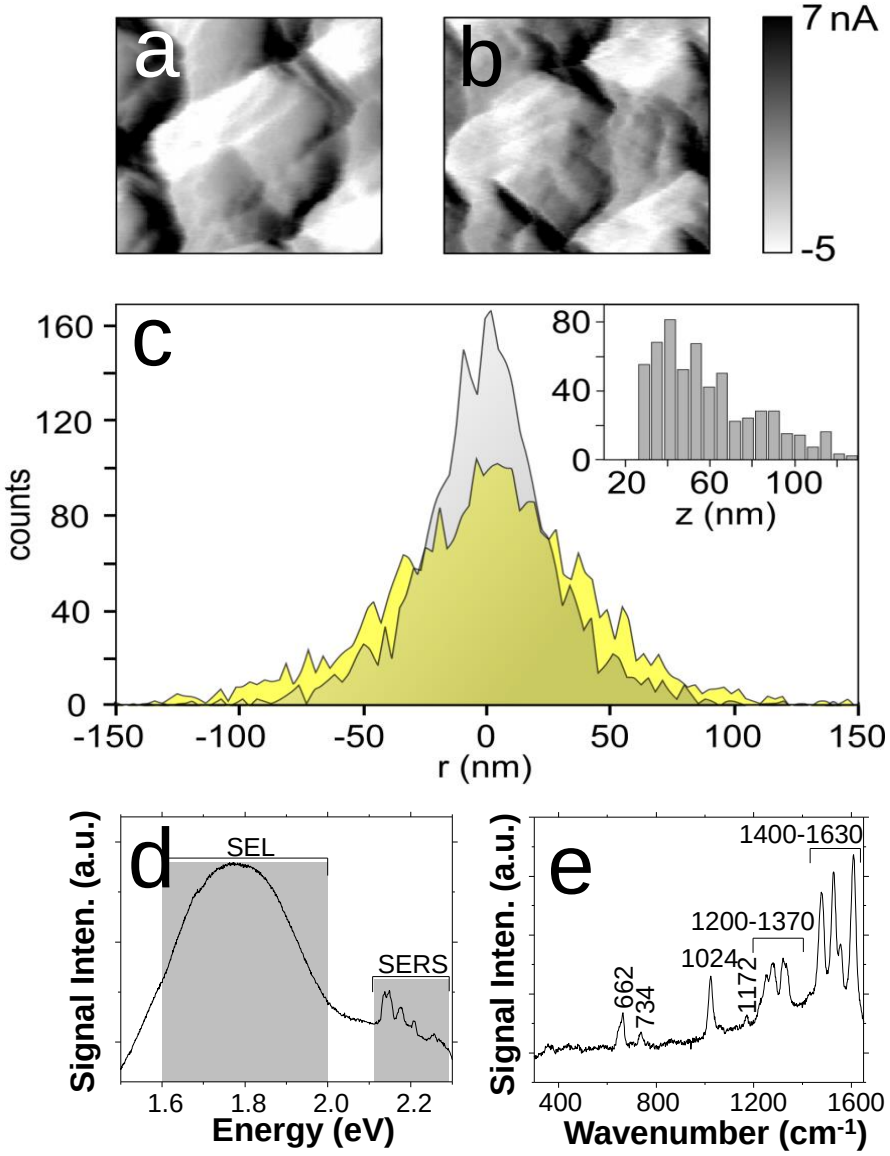

FIG. 2 Force gradient maps of (a) the unmodified array and (b) the modified array show a qualitative increase in roughness on the aggregate surface side.(c) The roughness histograms for 3000 randomly chosen points on the array alone (grey) and the array with aggregates (yellow). Inset: The distribution of aggregate heights. (d) Simultaneously recorded SERRS and SEL (e) SERRS spectrum shown in more detail with band positions marked. Spectra recorded at 532 nm.

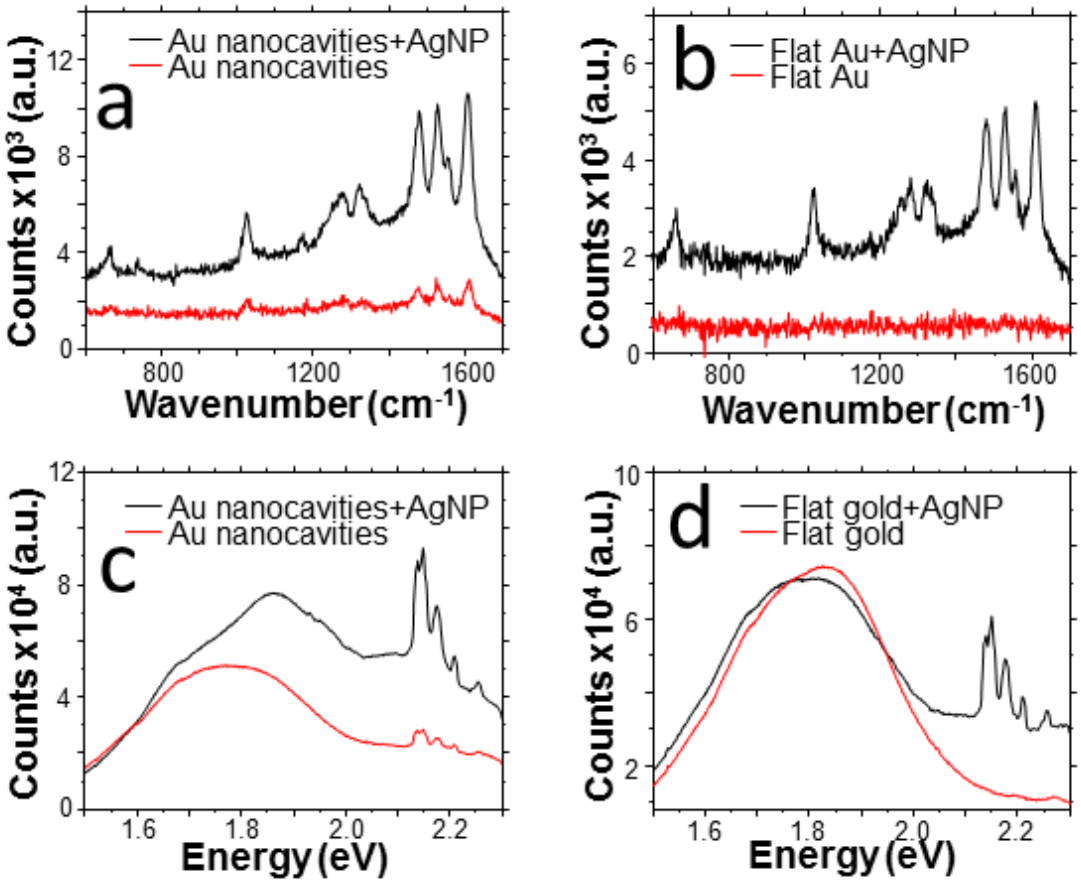

FIG. 3 SERRS spectra recorded from (a) Au nanocavity arrays and (b) flat gold both with and without NP deposition. SERRS and SEL spectra from (c) Au nanocavity arrays and (d) flat gold both with and without NP deposition.

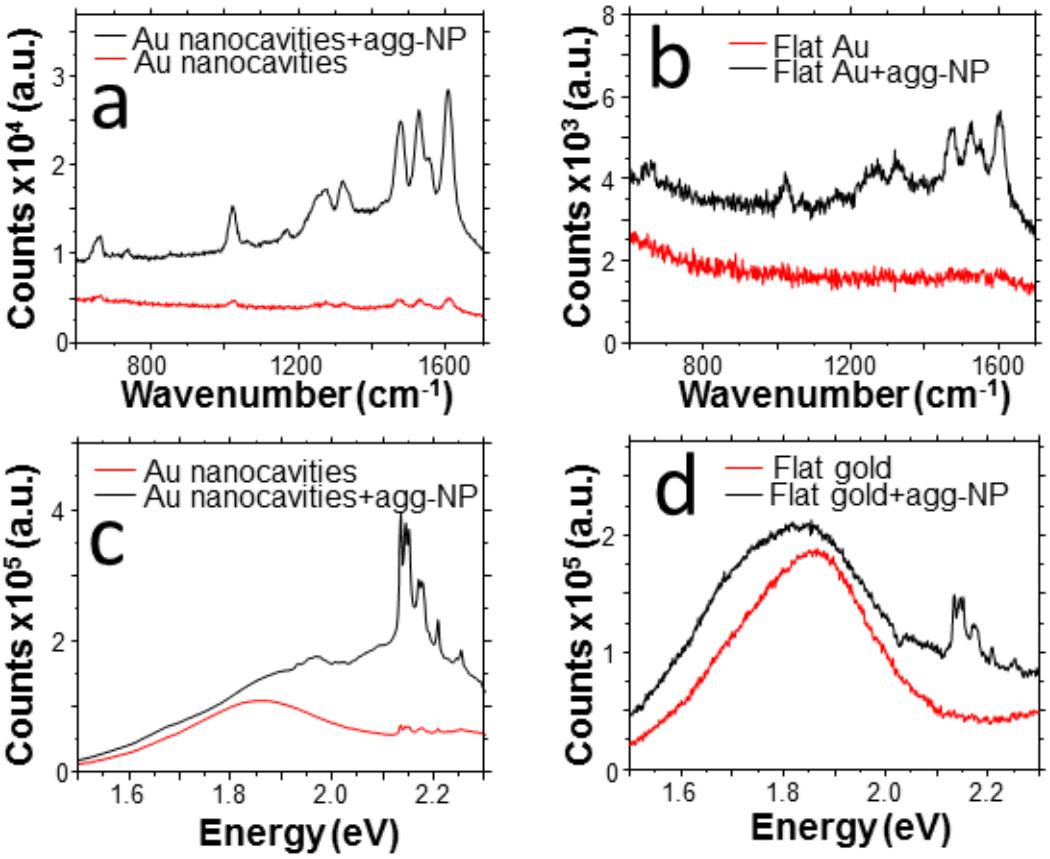

FIG. 4 SERRS and SEL spectra recorded from (a) Au nanocavity arrays and (b) flat gold both with and without NP deposition. SERRS and SEL spectra from (c) Au nanocavity arrays and (d) flat gold both with and without agg-NP deposition.

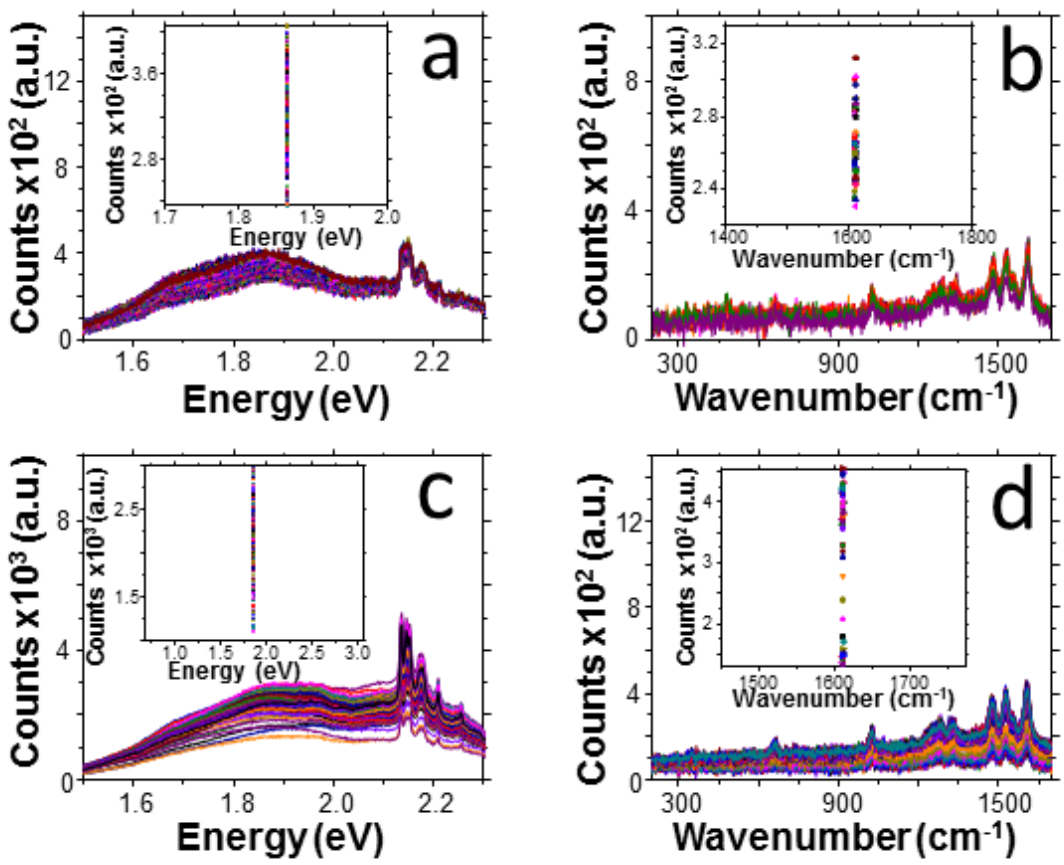

FIG. 5 (a) KS spectra of the SEL taken from the nanocavity array with deposited NPs. Inset: Plot of values of luminescence peak at 1.86eV showing how its value changes as the laser spot moves over the sample. (b) KS spectra of the SERRS taken from the nanocavity array with deposited NPs. Inset: Plot of values of the Raman peak at 1610cm^{-1} showing how its value changes as the laser spot moves over the sample. (c) KS spectra of the SEL taken from the nanocavity array with deposited agg-NPs. Inset: Plot of values of luminescence peak at 1.86eV showing how its value changes as the laser spot moves over the sample. (b) KS spectra of the SERRS taken from the nanocavity array with deposited agg-NPs. Inset: Plot of values of the Raman peak at 1610cm^{-1} showing how its value changes as the laser spot moves over the sample.

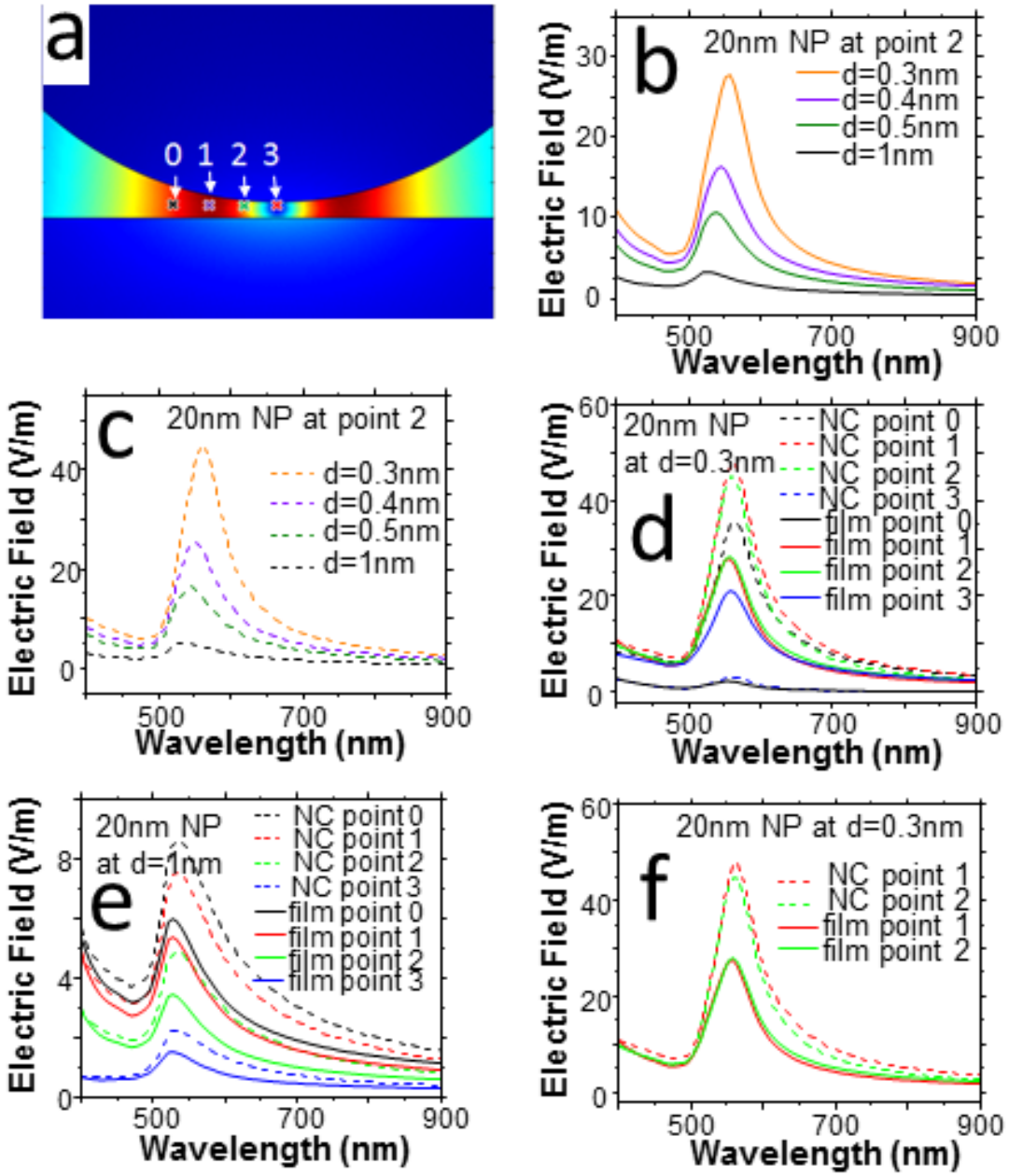

FIG. 6 COMSOL simulations of the electric field around a 20nm NP both in a nanocavity (diameter 600nm and height 150nm) in a gold nanovoid or on a gold film. Dashed lines represent NP in a nanovoid and unbroken lines represent the field strength when the NP is placed on a gold film. (a) Schematic drawing of a nanovoid with 20nm NP at different positions in the void, marked 0 to 3. (b) E-field plot at point 2 for different NP – film separation distance. (c) E-field plot o at point 2 for different NP – void separation distance. (d and e) E-field plots for NP in a void or on a film at two different separation distances for the flour points outlined in fig 6a. (f) Plots selected from (d) which show the configuration which gives the greatest electric field enhancement.

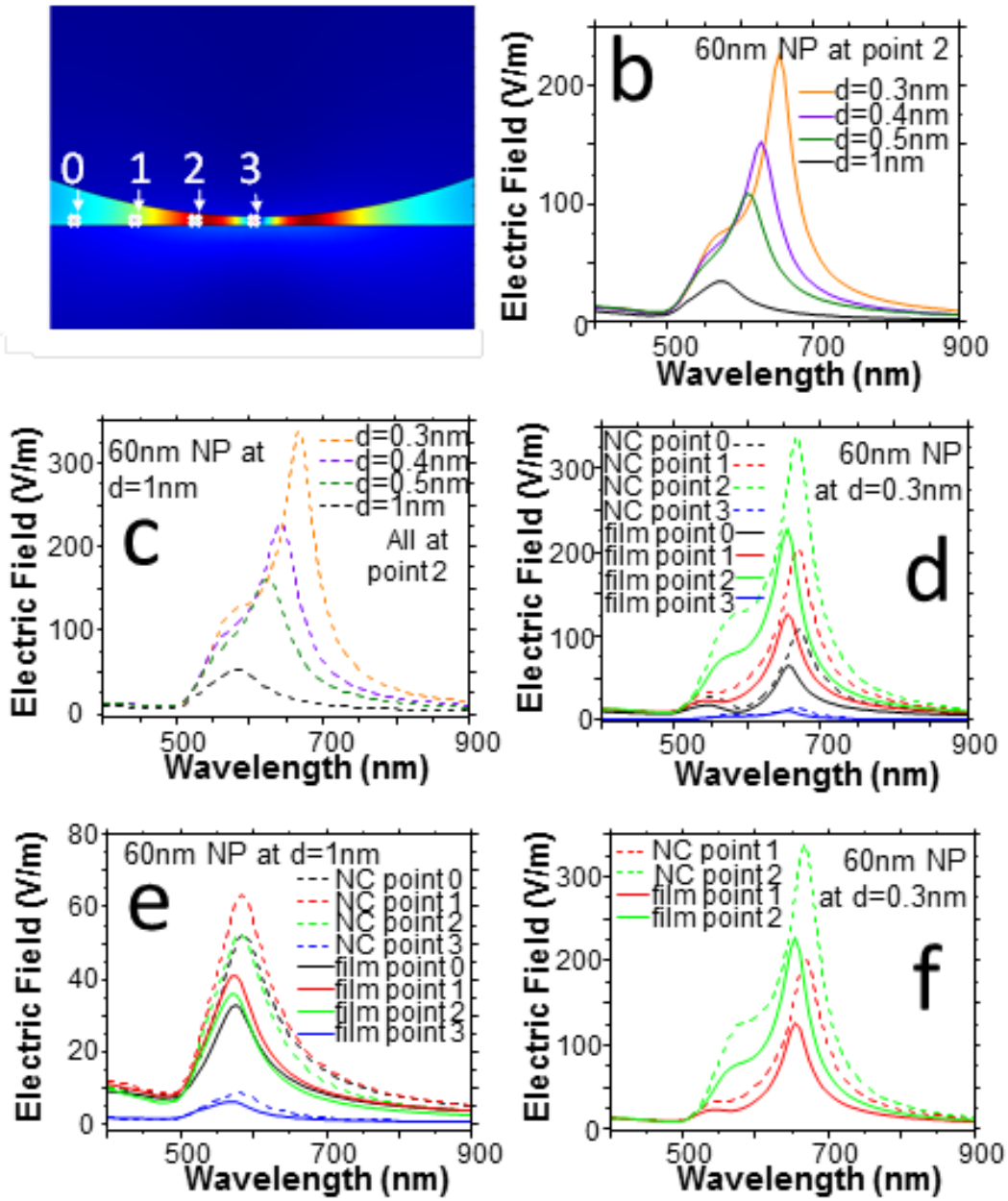

FIG. 7 COMSOL simulations of the electric field around a 60nm NP both in a nanocavity (diameter 600nm and height 150nm) in a gold nanovoid or on a gold film. Dashed lines represent NP in a nanovoid and unbroken lines represent the field strength when the NP is placed on a gold film. (a) Schematic drawing of a nanovoid with 20nm NP at different positions in the void, marked 0 to 3. (b) E-field plot at point 2 for different NP – film separation distance. (c) E-field plot o at point 2 for different NP – void separation distance. (d and e) E-field plots for NP in a void or on a film at two different separation distances for the flour points outlined in fig 7a. (f) Plots selected from (d) which show the configuration which gives the greatest electric field enhancement.